Mechanical properties of Ropaque hollow nanoparticles

*Liwen Zhu, Duc Nguyen, Tim Davey[#], Matthew Baker[#], Chris Such[#], Brian S. Hawkett, Chiara Neto**

School of Chemistry, Key Centre for Polymer and Colloids, and the Australian Institute for Nanoscale Science and Technology, The University of Sydney, NSW 2006 Australia

[#] DuluxGroup (Australia), 1970 Princess Highway, Clayton, Victoria 3168, Australia

* Corresponding author: Chiara.neto@sydney.edu.au

Abstract

The elastic properties and strength upon compression of commercial Ropaque polystyrene hollow particles were investigated by atomic force microscopy (AFM). These particles are commonly used in paints as opacifying agents, as their internal air void effectively scatters light. A sharp AFM tip was used to apply a point load to the particle surface, and increased to probe both the elastic and plastic deformation of the shell, and then further until the shell broke. For small deformations, the deformation increased linearly with applied force. The Young's modulus was calculated by accounting for the effect of the rigid substrate, and compare the modulus obtained from the Reissner and Hertz models. The minimum stress needed to destroy the integrity of the shell was extracted and found to be smaller than or close to that of silica hollow particles with different shell thickness tested in the literature.

Table of Contents graphic

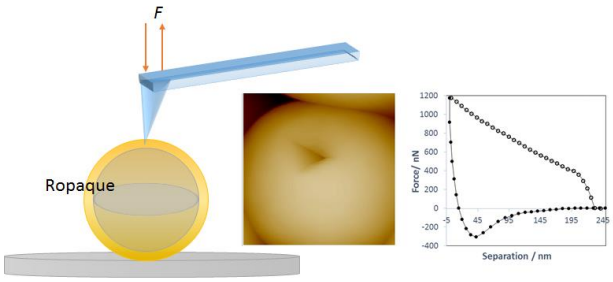

Keywords

Hollow particles, AFM, Mechanical properties

1. Introduction

Latex paints usually contain pigments that impart opacity and color, commonly inorganic particles such as TiO_2, and $CaCO_3$. As an alternative, hollow polymer particles are used as organic pigments. Ropaque™ particles are one such material made of cross-linked polystyrene with some acrylate, and commercialized by Dow Corning as opacifiers for water-based paints.[1] The use of Ropaque particles reduces the need for the environmentally costly TiO_2 particles, facilitates paint application and improves performance of paint, while reducing the cost of water-based paints. Ropaque™ particles are hollow and are filled with water in solution. During the drying process of the paint film, the water in the void diffuses through the polymer shell and leaves an air void.[2-3] Due to the difference in refractive index between air and the surrounding polymer, light is effectively scattered, contributing to the film opacity.[4] The particles size, particle size distribution and void fraction (44%) were designed to maximize the hiding efficiency.[2]

There are other requirements that paint additives such as Ropaque have to satisfy, an important one being their ability to withstand the stresses involved in the formation and application of the paint film and wear upon use. Ropaque particles are non-film forming,

which means they are designed to retain their hollow structure during film formation. Film formation is the process that occurs when a water-based latex paint is applied to the surface, and it entails a number of stages: as the water starts to evaporate from the film, the latex particles come into contact with each other, forming a close-packed array with water-filled interstices.[5] Then interstitial water evaporates, and particle deformation and compaction into dense arrays occurs. Finally, as the last of the water evaporates, the latex particles, which are film forming, i.e. above the glass transition temperature of the polymer, start to merge into a homogeneous, continuous film; at this stage the film would appear optically transparent. With the addition of Ropaque particles, which are now filled with air, the film becomes opaque.

In this paper we investigate the mechanical properties of Ropaque polymer particles using atomic force microscopy (AFM) force-indentation curves. As the stiffness of the polymer shells is expected to increase with shell thickness, we measure the mechanical properties of Ropaque, which are relevant to their ability to withstand the typical stresses involved in the paint drying process, and also upon exposure to man-induced wear of the paint film. AFM used as a nano-indenter allows characterization of single nanoparticles. Over the last 20 years, it has been used to study the mechanical properties of various systems such as thin polymer films,[6-7] microcapsules,[8-14] vesicles,[15-16] polymer microspheres,[17-18] nanotubes,[19] and cells.[20] Despite Ropaque particles being heavily used in paints, only a few studies are present in the literature on their properties (optical[4] and rheological[21]), and their mechanical properties on the nanoscale have not been characterized.

Our study benefits a wider range of materials of fundamental and applied relevance, for example nanoscale polymer capsules used as drug carriers which should be designed to burst (for example under the stimulus of a change in environmental conditions)[22] and deliver the drug to a target tissue. Microcapsules filled with liquid are often used for encapsulation and delivery of flavors, scents and nutrients in the food, pharmaceutical and agricultural

industry.[23] In all these applications, knowledge of the mechanical properties of the capsules is crucial to the control over the timing and the stimulus of the release of their cargo. In addition, knowledge of the force required to deform hollow polymer particles is beneficial to inform the typical forces required to image these particles by AFM with minimal deformation, reducing therefore artifacts in size measurements.

2. Materials and Methods

For microscopic characterization, a suspension of Ropaque^{TM} Ultra particles (Dow Chemical Co.) was deposited onto silicon substrates by spin-coating. Scanning electron microscopy (Zeiss Sigma HD FEG SEM) was used to characterize the sphere size and surface roughness, and transmission electron microscopy (TEM, Philips CM120 Biofilter) was used to measure the shell thickness. Tapping-mode AFM imaging and force measurements were performed with a Multimode Nanoscope 8 (Bruker) at room temperature using Multi75Al-G and Tap300Al-G silicon AFM probes (BudgetSensors, nominal tip radius 10 nm). The spring constant of each cantilever was determined by using the Sader method knowing the geometry of the cantilever.[24] To determine the elastic contribution to the mechanical properties, force-distance curves were collected on the individual particles. Before starting the force measurements, the Ropaque particles were imaged in tapping mode, and a well-shaped particle was chosen. By repeatedly zooming in, the AFM tip was carefully located on the top of the target particle. A series of force measurements were collected, whereby the applied force was gradually increased to induce increasing deformation. The elastic modulus of the particle was determined by AFM force-distance curves at low values of deformation.

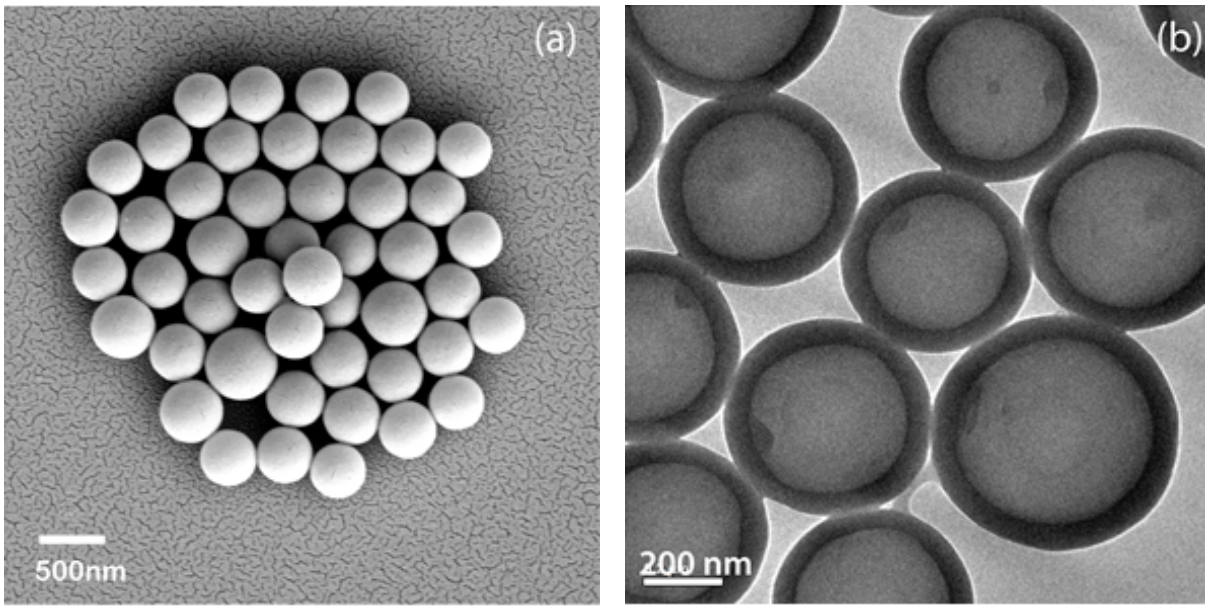

Figure 1. (a) SEM and (b) TEM micrographs of the Ropaque^{TM} particles used in this study.

3. Results and Discussion

As shown in Figure 1(a), Ropaque particles are regular and spherical in shape, the particle size distribution is fairly narrow, and the average size measured from the SEM image is 423 ± 21 nm. The polymer shell thickness, as evidenced in Figure 1(b), is also uniform and reproducible and measures 40 ± 5 nm. These values correspond well with the reported values for Ropaque particles.[2] The tips used for indentation are pyramidal in shape. There was no obvious sign of the AFM tip becoming blunt upon indention on the Ropaque particles. However, after the tip was driven at high loads through the particle and to hard contact with the silicon wafer, evidence of tip blunting was seen in the subsequent AFM images (see Figure S1).

3.1 Nano-indentation by AFM

In the AFM nanoindentation force measurement, the tip was driven vertically towards the top of a particle, and when it touched the particle at a constant velocity, the deflection of the AFM cantilever was recorded. The deflection was then converted into a force by knowledge

of the spring constant.[25-26] The sensitivity of the cantilever was obtained on a hard sapphire surface before or after the force measurements, and was used to convert deflection signal to force with the cantilever spring constant. The aim of this experiment was to control the force applied to the particle shell to obtain the Young's modulus of the shell and the minimum force required to break the shell.

Based on established literature,[27] during the force loading, the elastic deformation is entirely recoverable once the applied force is removed. If the loading force is increased beyond a certain limit, the material either fails to return to its original form when the force is removed due to the plastic deformation, or the material shatters into fragments.

In our experiments, firstly Ropaque particles were imaged by tapping mode AFM. A clean and regular single particle was imaged by tapping mode AFM (as shown in Figures 2(a) and (b)), and a single force measurement was performed in the center (top) of the selected particle. By controlling the piezo driving distance and the trigger threshold of the cantilever deflection, the amount of loading force was controlled. After each single force measurement, the target particle was imaged again as shown in Figures 2(c) and (d). The ability of the tip to image the sample clearly after indentation indicated that the tip shape was not significantly damaged by the contact. Evidence of tip indentation on the particle shell could be observed when plastic deformation was sufficiently large, and was particularly clear in the phase AFM micrographs (Figure 2(d)), and more subtle in the topography micrographs (Figure 2(c)).

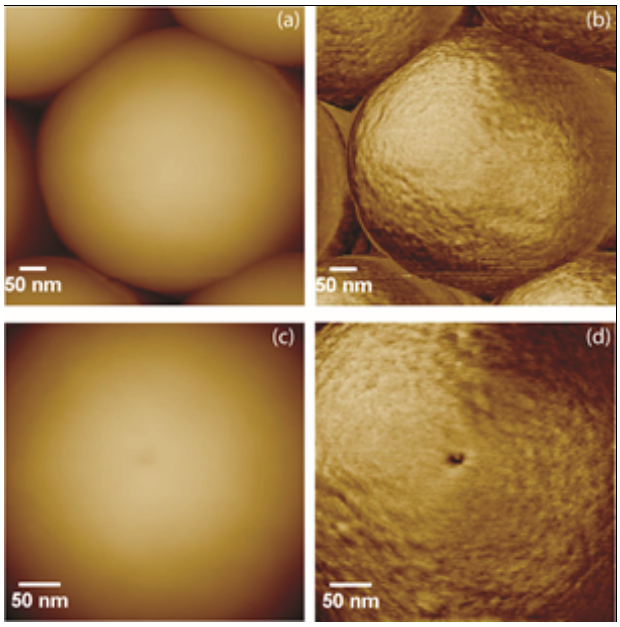

Figure 2. Tapping mode AFM micrographs of the Ropaque particles, before a force measurement (a and b), and after a force measurement that led to a plastic deformation (c and d). (a) and (c) are AFM topography micrographs and (b) and (d) are phase micrographs.

3.2 Force versus deformation in the elastic limit

Force measurements on the Ropaque particles were obtained and converted into force versus separation curves using an established method,[25] and representative data is shown in Figures 3-6. For low loading forces up to around 50 nN (corresponding to approximately 1.59×10^{8} Pa = force / area of contact, using the nominal tip radius 10 nm), a soft cantilever was used (Multi75Al-G AFM probe, spring constant ~ 3 N/m), and the experiment can be assumed to be entirely in the elastic limit, as discussed below. In Figure 3 at tip-sample separations > 5 nm, the tip does not touch the particle so the measured force is zero. When tip – particle separation becomes < 5 nm, an attractive interaction was measured (at separation 3 - 4 nm, corresponding to negative values of the force), followed by a repulsive force, and followed by the compliance region, where the tip and the particle are in hard contact. In first instance, the maximum force applied was kept low, below 50 nN, to maintain low values of sample deformation. In Figure 3(a), the approach (open circles) and withdraw force curves

(solid circles) overlap; the absence of hysteresis in the force loop is an indication that the deformation is within the elastic limit.[11]

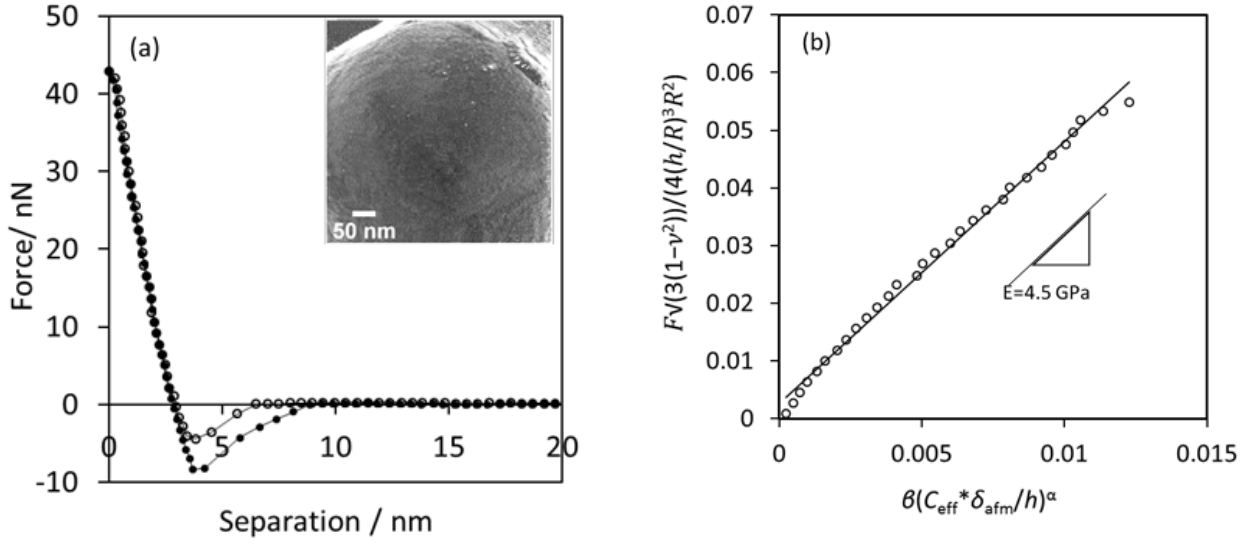

Figure 3. (a) A typical force curve on a Ropaque particle with a shell thickness of 40 nm and a diameter of ~ 400 nm, within the elastic limit. The open circles denote the approach curve, and the filled circles denote the withdraw part of the curve. The inset image is an AFM phase image obtained on the center of the particle after this single force measurement. (b) The corresponding normalised force-indentation curve extracted from the withdraw curve in Figure 3(a), presented in the form given by Equation 3. The Young's modulus of the material property is the slope of solid line, the fitted value E = 4.5 GPa in this example.

The elastic modulus of thin-shelled capsules can be calculated using the Reissner model,[28] while that of solid particles using the Hertz model.[29] As the Reissner Equation is appropriate for hollow capsules with a shell thickness to capsule radius ratio $h/R < 1/20$,[30] and the Ropaque particles have a ratio $h/R \sim 1/10$, it is useful to compare the results from both models. For a given indentation δ (less than the shell thickness h), the force F on a thin

capsule shell of radius *R,* Poisson's ratio *v,* and Young's modulus *E* according to Reissner's formula is:

$$F = \frac{4Eh^2\delta}{R\sqrt{3(1-v^2)}} \qquad (1)$$

In the case of a solid particle of radius *R*, the Hertz[29] model is:

$$F = \frac{4}{3}\frac{E}{(1-v^2)}\,\bar{R}^{0.5}\,\delta^{1.5} \qquad (2)$$

Where $\bar{R} = R_P R/(R_P + R)$ is the effective radius, R_p is the radius of the AFM tip (nominal 10 nm) and *R* is the Ropaque particle radius (400 nm).

The withdraw curve was fitted using both the Reissner model (Equation 1) and the Hertz model (Equation 2) in order to extract the Young's modulus *E*. The Poisson's ratio of Ropaque particles, which are mainly cross-linked polystyrene with some acrylate, is not known, so the value for bulk polystyrene (v = 0.33)[17] was used. The employed AFM tip have a bulk elastic modulus of 130 - 160 GPa,[17] and as this value is expected to be much larger than that of Ropaque particles, we assumed that the AFM tip did not deform. The average Young's modulus of the Ropaque particles obtained from the basic Reissner model (Equation 1) was 0.9 ± 0.2 GPa model and from the basic Hertz model (Equation 2) was double this, 1.9 ± 0.1 GPa. Both values were obtained from 15 force measurements on different Ropaque particles.

To further improve this estimate, and following recent work by Berry *et al.*[31], the additional effect of the rigid substrate under the particle could be estimated. The compression of the particle leads to deformation at both the top of the particle and at the bottom adjacent to the substrate. However, the AFM measurement does not provide sufficient information to distinguish the substrate effect. Thus, the indentation measured by the AFM cantilever δ_{afm} is

the sum of both the particle indentation at the substrate and the effective indentation δ_{eff} on the top of the particle due to the AFM tip.

The correction factor C ($C = \delta_{eff}/\delta_{afm}$) that accounts for the substrate indentation was derived in references[31-32] for soft particles ($h/R = 1$, h is the thickness of the particle shell) in terms of the indenter to particle radius ratio R_p/R. Berry *et al.*[31] characterized the correction factors for capsules with $h < R$ by numerical simulations over the range of shell thickness.

Using the effective indentation δ_{eff} rather than the AFM measured indentation δ_{afm} in the Reissner and Hertz models and combining appropriate correction factors (scaling coefficient β and scaling exponent α), Berry *et al.*[31] provided a general expression to include the substrate effect from thin shell capsule indentation (Reissner solution) to solid particle indentation (Hertz solution), as shown in Equation 3. The parameters C, β and α are functions of the experimental parameters Poisson's ratio v, the AFM tip radius ratio R_p/R, and the shell thickness ratio h/R. The values can be determined using numerical simulations.[31]

$$\frac{F\sqrt{3(1-\nu^2)}}{(h/R)^3 4R^2} = E\beta\left(\frac{C\delta_{afm}}{h}\right)^{\alpha} \qquad (3)$$

Using Berry's Equation (Equation 3), the Young's modulus of Ropaque particles can be calculated from experimental force-indentation data with the correction factor C (0.69), the scaling exponent α (1.38) and the scaling coefficient β (0.77). In Figure 3(b), we show an example of experimental force-indentation data extracted from Figure 3(a), presented in the form given by Equation 3. The fitted average Young's modulus of the hollow Ropaque particle obtained from 15 force measurements on different Ropaque particle is 5.0 ± 0.4 GPa using Equation 3. The Young's modulus obtained from Equation 3 is higher than the ones obtained by fitting the basic Reisser model (E = 0.9 ± 0.2 GPa) and basic Hertz model (E = 1.9 ± 0.1 GPa), and probably a better estimate of the actual modulus of the shell; the value is in good agreement with the Young's modulus for polystyrene in literature in the range of 2.4 ~ 5 GPa.[33]

3.3 Force versus Deformation in the plastic region

When the maximum loading force applied was increased to around 100 - 150 nN, the withdraw curves no longer overlapped with the approach curves, and this hysteresis in the contact region is associated with plastic deformation.[11] The extent of the plastic deformation was estimated by the separation between the two intercepts of the approach and withdraw curves with the $y = 0$ axis, as shown by the line between points A and B in Figure 4(a). Figure 4(b) shows three force curves taken on three different particles at increasing loading force. After each force measurement, the particles were imaged again (as shown in the inset of the Figure 4(a)). The plastic deformation increased with the increase of the loading force, and in this regime the deformation of the particles was maintained to less than 40 nm, i.e. below the thickness of the shell.

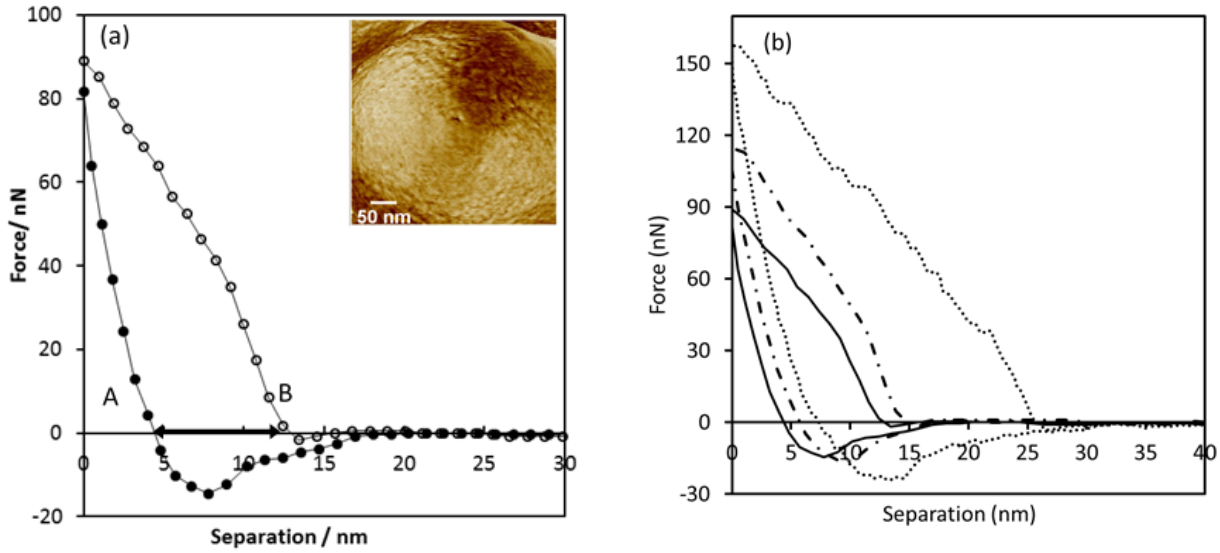

Figure 4. Force-distance curves obtained at maximum loading force around 150 - 200 nN, showing plastic deformation. (a) A single force–distance curve, the distance between points A and B is used as a measure of plastic deformation. Inset: AFM phase image obtained after the force measurement. (b) Three force-distance curves with increasing maximum loading force.

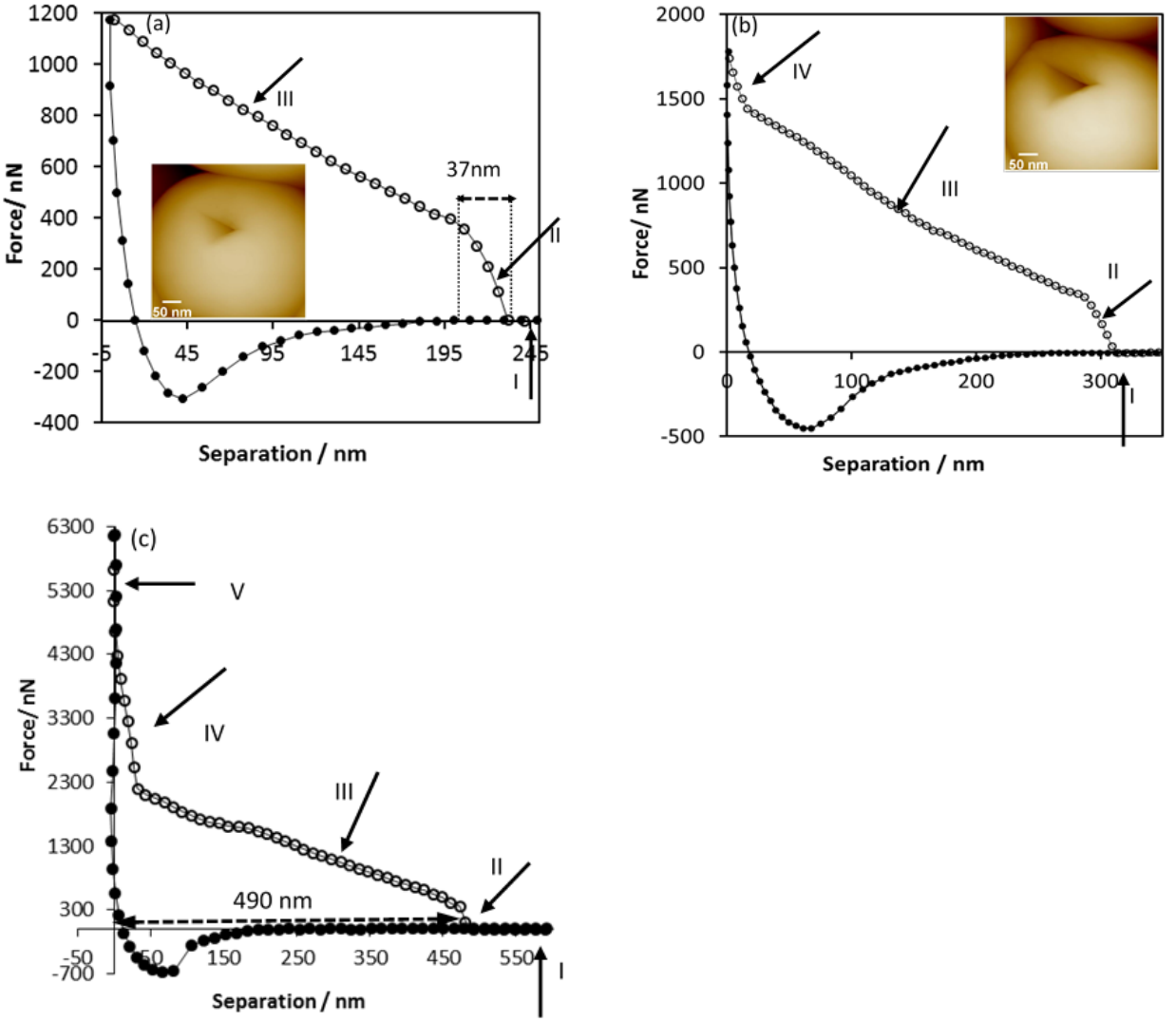

Figure 5. AFM force-separation curves obtained while gradually increasing loading force (empty circles represent an approach curve, full circles represent a withdraw curve). The insets are AFM topography micrographs obtained after each force measurement. (a) At maximum loading force around 400 nN, the tip has pierced through the top shell. (b) At maximum loading force around 1500 – 2000 nN, the tip has pierced through the particle shell and touched the bottom shell. (c) At maximum loading force > 4500 nN, the tip has reached the hard contact with the silicon substrate under the particle.

As the Ropaque particles are hollow particles, when the loading force was increased further, the tip pierced through the particle shell. In Figure 5(a), a large hysteresis can be

seen between the approach and withdraw curves, and the approach curve shows three different regions with different slopes. The first region (**I**) is the baseline corresponding to zero force, which is flat. In the second region (**II**) the slope is high and caused by the tip pressing into the shell and penetrating the shell. The distance spanned by the region **II** is about 37 nm which is close to the shell thickness. The third region (**III**) with a lower slope is caused by the tip pushing through the shell and increasing the indentation mark. The inset highlights the large indent in the target Ropaque particle scanned after this force measurement.

As the loading force was further increased to 1500 – 2000 nN, an additional (**IV**) region, with a higher slope, appeared in the approach curve at short separations (Figure 5(b)), caused by the tip indenting on the bottom shell of the particle, resting on the substrate. Finally, at even higher loads (5000 - 6000 nN), a fifth (**V**) region with the highest slope appeared (Figure 5(c)), caused by contact of the tip with the hard silicon substrate under the particle. In this region, the approach and withdraw curves coincide. In the latter force curve, the diameter of the particle could be estimated to be 490 nm, which is close to the value measured by SEM. The average slopes of the approach force curves in the different force regions **II**, **III** and **IV** are summarized in Table 1.

Region	II	III	IV
Slope (N/m)	14.3	3.6	78.6
Standard deviation	8.7	0.8	10.1

Table 1. The average slopes of the approach curves in the three different regions, averaged over 34 curves for slope **II**, 12 curves for slope **III** and 3 curves for slope **IV**.

In separate experiments, the same high loading force (6000 - 7000 nN) was applied repeatedly at the same position on a particle, as shown in Figure 6. In this set, only the first force curve presented all five regions of different slopes. In the following curves, the three regions of slope **II**, **III** and **IV** have merged into a smooth curve at lower force values in the approach curve, as the first force curve has induced a permanent plastic deformation on the shell. In this case, the repeated force curves had the effect of enlarging the existing indentation. The small amount of repulsive force shown in the approach curve prior to hard contact is likely due to the friction from the broken shell acting on the side of AFM tip.

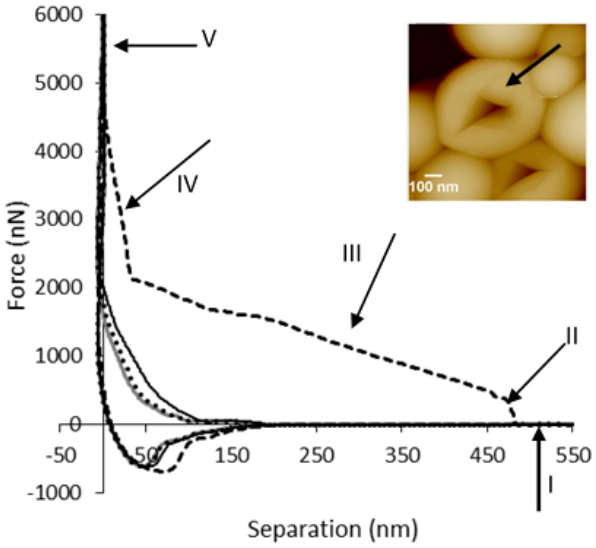

Figure 6. Four AFM force-separation curves obtained at the same loading force in the same position of the particle. The inset is an AFM topography micrograph obtained after the fourth force measurement. The target particle is market by the arrow. The dashed curve represents the first force measurement. The black solid curve represents the following second force measurement. The dotted curve represents the third force measurement. The grey solid curve represents the last force measurement.

3.4 Typical stress applied to Ropaque particles

A summary of indentation versus loading force, including data from 19 single force measurements, is shown in Figure 7. Indentation increases approximately linearly as the force is increased. The variability in the deformation values are probably due to slightly different loading positions on different target particles while recording force curves. By interpolation from the line of best fit to this data, the force required to induce a 40 nm indentation can be extracted and is ≥ 390 nN (the average shell thickness is 40 nm). Therefore, the minimum stress for breaking the shell of the Ropaque hollow particle with a point force could be roughly calculated by dividing this force (390 nN) by the cross-sectional area of the tip (nominal tip radius is 10 nm). The calculated breaking stress is then about 1.2 GPa. In the work by Zhang *et al.,* [11] the breaking stress for 800 nm large hollow silica spheres with shell thickness 23 nm was about 3 GPa. In Yue *et al*'s work,[34] the breaking stress for an ultrathin hollow silica sphere (sphere radius R = 400 nm, the shell thickness was 12 nm) was about 2.1 GPa. It is perhaps surprising that the breaking stress of the polystyrene Ropaque hollow particle is relatively close to that of ultrathin silica spheres. The point force measurements conducted here might be used by other researchers to benchmark the robustness of custom-synthesized shells, and therefore predict their potential success in applications.

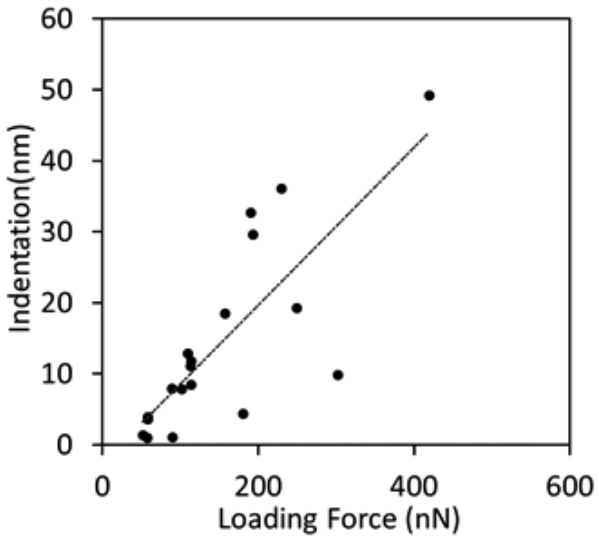

Figure 7. Indentation versus loading force, as obtained from 19 individual force measurements (solid circles). The dotted line is a line of best fit, and R^2 for the fit is 0.62. Then equation for the fit is $y = 0.11\ x - 2.54$.

Although the Ropaque particles are not as strong as the hollow silica particles, they are relatively stable to elastic and plastic shell deformation by point force loads, up to stresses around 2×10^8 Pa. During the paint drying process, the latex particles coalesce and deform to form an integral film. Many theories have been proposed to account for the origin of the deformation forces experienced by the particles during film formation, such as capillary theory[35], JKR theory[36] and other theories[37-38]. The magnitude of the typical deformation stresses during drying were found to be in the range of 10^6 to 10^8 Pa in the literature,[35-38] values close to the Ropaque breaking stress. This result demonstrates that Ropaque particles are engineered with a shell sufficiently strong to withstand the typical stresses in paint film formation.

4. Conclusions

We have measured the elastic properties and the stress required for breaking through Ropaque hollow particles, which have a radius of 400 nm and a shell thickness of 40 nm. By conducting point force measurements, we have calculated the Young's modulus of Ropaque shells with three different methods. The Hertz model and Reissner model tend to underestimate the Young's modulus of hollow particles by neglecting the effect of the rigid substrate, while the Berry model taking the substrate into account estimates a Young's modulus of 5 GPa, compatible with bulk polystyrene values. From our force measurements, the Ropaque cross-linked polystyrene shells appear to be robust enough to prevent shell breakage due to the typical stresses involved in the paint dry process. The knowledge of the stress at breaking point by point force measurements is useful to engineer efficient micro- and

nano-capsules that release active components, and to quantify the required trigger for the intended application.

Supporting Information

Description: SEM images of a blunt AFM tip before and after the tip was driven at high loads through the particle and to hard contact with the silicon wafer.

Acknowledgements

The authors thank Dr Joseph Berry and Dr Michael Kappl for useful discussions. We acknowledge funding from the Australian Research Council and DuluxGroup Australia through Linkage grant LP140100285.

References

1. Kowalski, A.; Vogel, M. Process for making multistage polymer particles, product thus obtained, process for making aqueous dispersions of these particles, product thus obtained, process for making films, compositions for coating and/or impregnating, multistage polymers and their use. EP 0022633 A2, 1981.

2. Dow Corning *ROPAQUE™ ULTRA E Opaque Polymer*; Technical Data Sheet; 2013.

3. Association, A. O. C. C. *Surface coatings*. The New South Wales University Press: 1983; Vol. 1.

4. Auger, J.-C.; McLoughlin, D. Theoretical study and experimental analysis of the scattering efficiency of hollow polymer particles in the dependent light scattering regime. *J. Coat. Technol. Res.* **2015,** *12*, 693-709.

5. Reddie, J. L.; Meredith, P.; Jones, R. A. L.; Donald, A. M. Kinetics of Film Formation in Acrylic Latices Studied with Multiple-Angle-of-Incidence Ellipsometry and Environmental SEM. *Macromolecules* **1995,** *28*, 2673-2682.

6. Vanlandingham, M. R.; McKnight, S. H.; Palmese, G. R.; Elings, J. R.; Huang, X.; Bogetti, T. A.; Eduljee, R. F.; Gillespie, J. W. Nanoscale indentation of polymer systems using the atomic force microscope. *J. Adhes.* **1997,** *64*, 31-59.

7. Du, B.; Tsui, O. K. C.; Zhang, Q.; He, T. Study of Elastic Modulus and Yield Strength of Polymer Thin Films Using Atomic Force Microscopy. *Langmuir* **2001,** *17*, 3286-3291.

8. Vinogradova, O. I.; Lebedeva, O. V.; Kim, B.-S. Mechanical behavior and characterization of microcapusles *Annu. Rev. Mater. Res.* **2006,** *36*, 143-178.

9. Lisunova, M. O.; Drachuk, I.; Shchepelina, O. A.; Anderson, K. D.; Tsukruk, V. V. Direct Probing of Micromechanical Properties of Hydrogen-Bonded Layer-by-Layer Microcapsule Shells with Different Chemical Compositions. *Langmuir* **2011,** *27*, 11157-11165.

10. Glynos, E.; Sboros, V.; Koutsos, V. Polymeric thin shells: Measurement of elastic properties at the nanometer scale using atomic force microscopy. *Mater. Sci. Eng. B* **2009,** *165*, 231-234.

11. Zhang, L.; D'Acunzi, M.; Kappl, M.; Auernhammer, G. K.; Vollmer, D.; van Kats, C. M.; van Blaaderen, A. Hollow Silica Spheres: Synthesis and Mechanical Properties. *Langmuir* **2009,** *25*, 2711-2717.

12. Zhang, L.; D'Acunzi, M.; Kappl, M.; Imhof, A.; Blaaderen, A. v.; Butt, H.-J.; Graf, R.; Vollmer, D. Tuning the mechanical properties of silica microcapsules. *PCCP* **2010,** *12*, 15392-15398.

13. Fery, A.; Weinkamer, R. Mechanical properties of micro- and nanocapsules: Single-capsule measurements. *Polymer* **2007,** *48*, 7221-7235.

14. Mettu, S.; Zhou, M.; Tardy, B. L.; Ashokkumar, M.; Dagastine, R. R. Temperature dependent mechanical properties of air, oil and water filled microcapsules studied by atomic force microscopy. *Polymer* **2016,** *102*, 333-341.

15. Liang, X.; Mao, G.; Ng, K. Y. S. Mechanical properties and stability measurement of cholesterol-containing liposome on mica by atomic force microscopy. *J. Colloid Interface Sci.* **2004,** *278*, 53-62.

16. Chen, Q.; Schonherr, H.; Vancso, G. J. Mechanical properties of block copolymer vesicle membranes by atomic force microscopy. *Soft Matter* **2009,** *5*, 4944-4950.

17. Tan, S.; Sherman, R. L.; Ford, W. T. Nanoscale Compression of Polymer Microspheres by Atomic Force Microscopy. *Langmuir* **2004,** *20*, 7015-7020.

18. Chen, Y.; Qian, C.; Miao, N. Atomic force microscopy indentation to determine mechanical property for polystyrene–silica core–shell hybrid particles with controlled shell thickness. *Thin Solid Films* **2015,** *579*, 57-63.

19. Qi, H. J.; Teo, K. B. K.; Lau, K. K. S.; Boyce, M. C.; Milne, W. I.; Robertson, J.; Gleason, K. K. Determination of mechanical properties of carbon nanotubes and vertically aligned carbon nanotube forests using nanoindentation. *J. Mech. Phys. Solids* **2003,** *51*, 2213-2237.

20. Thomas, G.; Burnham, N. A.; Camesano, T. A.; Wen, Q. Measuring the Mechanical Properties of Living Cells Using Atomic Force Microscopy. *J. Visualized Exp.* **2013**, 50497.

21. Feng, J.; Odrobina, E.; Winnik, M. A. Effect of Hard Polymer Filler Particles on Polymer Diffusion in a Low-Tg Latex Film. *Macromolecules* **1998,** *31*, 5290-5299.

22. De Geest, B. G.; Sanders, N. N.; Sukhorukov, G. B.; Demeester, J.; De Smedt, S. C. Release mechanisms for polyelectrolyte capsules. *Chem. Soc. Rev.* **2007,** *36*, 636-649.

23. Nedovic, V.; Kalusevic, A.; Manojlovic, V.; Levic, S.; Bugarski, B. An overview of encapsulation technologies for food applications. *Procedia Food Sci.* **2011,** *1*, 1806-1815.

24. Sader, J. E.; Chon, J. W. M.; Mulvaney, P. Calibration of rectangular atomic force microscope cantilevers. *Rev. Sci. Instrum.* **1999,** *70*, 3967-3969.

25. Senden, T. J. Force microscopy and surface interactions. *Curr. Opin. Colloid Interface Sci.* **2001,** *6*, 95-101.

26. Zhu, L.; Attard, P.; Neto, C. Reliable Measurements of Interfacial Slip by Colloid Probe Atomic Force Microscopy. I. Mathematical Modeling. *Langmuir* **2011,** *27*, 6701-6711.

27. Fischer-Cripps, A. C. *Nanoindentation*. Springer: New York, 2002.

28. Reissner, E. Stresses and Small Displacements of Shallow Spherical Shells .2. *J Math Phys Camb* **1946,** *25*, 279-300.

29. Hertz, H. On the contact of elastic solids. *J. Reine. Angew. Math* **1982,** *92*, 156–171.

30. Gregory, R. D.; Milac, T. I.; Wan, F. Y. M. A thick hollow sphere compressed by equal and opposite concentrated axial loads: An asymptotic solution. *Siam J Appl Math* **1999,** *59*, 1080-1097.

31. Berry, J. D.; Mettu, S.; Dagastine, R. R. Precise measurements of capsule mechanical properties using indentation. *Soft Matter* **2017,** *13*, 1943-1947.

32. Glaubitz, M.; Medvedev, N.; Pussak, D.; Hartmann, L.; Schmidt, S.; Helm, C. A.; Delcea, M. A novel contact model for AFM indentation experiments on soft spherical cell-like particles. *Soft Matter* **2014,** *10*, 6732-6741.

33. Cappella, B. *Mechanical Properties of Polymers Measured through AFM Force-Distance Curves*. Springer: Germany, 2016.

34. Yue, Q.; Li, Y. Z.; Kong, M.; Huang, J. C.; Zhao, X. J.; Liu, J.; Williford, R. E. Ultralow density, hollow silica foams produced through interfacial reaction and their exceptional properties for environmental and energy applications. *J. Mater. Chem.* **2011,** *21*, 12041-12046.

35. Brown, G. L. Formation of Films from Polymer Dispersions. *J. Polym. Sci.* **1956,** *22*, 423-434.

36. Kendall, K.; Padget, J. C. Latex coalescence. *Int. J. Adhes. Adhes.* **1982,** *2*, 149-154.

37. Kan, C. S. Role of particle size on latex deformation during film formation. *J Coating Technol* **1999,** *71*, 89-97.

38. Sheetz, D. P. Formation of Films by Drying of Latex. *J. Appl. Polym. Sci.* **1965,** *9*, 3759-3773.